Available online at www.eccomasproceedia.org
Eccomas Proceedia COMPDYN (2017) 1711-1731

ECCOMAS
Proceedia

COMPDYN 2017
6th ECCOMAS Thematic Conference on
Computational Methods in Structural Dynamics and Earthquake Engineering
M. Papadrakakis, M. Fragiadakis (eds.)
Rhodes Island, Greece, 15–17 June 2017

SIMULATION OF MONOTONIC, STATIC AND DYNAMIC RESPONSE OF RC SQUAT WALLS BY MEANS OF PARC_CL 2.0 CRACK MODEL

Beatrice Belletti*, Matteo Scolari* and Francesca Vecchi*
Università degli Studi di Parma, Dipartimento di Ingegneria Civile, Ambiente e Territorio e Architettura DICA-TeA, Parco area delle Scienze 181/A, 43124, Parma (ITALY)

Keywords: non-linear finite element analyses, shear walls, PARC_CL crack model

Abstract. *In this paper the PARC_CL 2.0 crack model, implemented in the ABAQUS Code user subroutine UMAT.for, is presented and applied to the non-linear finite element analyses (NLFEA) of reinforced concrete (RC) shear walls tested, by means of pseudo dynamic test (PSD), at the European Laboratory for Structural Assessment (ELSA, Joint Research Centre).*

The PARC_CL 2.0 crack model is an evolution of the previous PARC versions and, with respect to them, it allows to take into account plastic and irreversible deformations. For this reason, it seems to be suitable for modelling the hysteretic cycles of both concrete and steel and to reproduce the cyclic response of structural R members. Moreover, within the PARC_CL 2.0 crack model, is implemented a formulation able to account for stiffness proportional damping in dynamic analyses.

The shear walls, tested by means of PSD test, at the ELSA laboratory have been used to validate the proposed PARC_CL 2.0 crack model; the shear walls have been modeled using multi-layered shell elements and NLFEA have been carried out considering several loading condition (static pushover, cyclic and dynamic). The static pushover analyses are used to evaluate the sensitivity of results to mesh discretization; several analyses have been carried out adopting different element size in order to see the effect on the structural response.Moreover, cyclic and dynamic analyses are used to evaluate the capability of PARC_CL 2.0 crack model to reproduce the hysteretic response of such RC structural members.

Peer-review under responsibility of the organizing committee of COMPDYN 2017.
doi: 10.7712/120117.5524.18761

1 INTRODUCTION

Structural reinforced concrete (RC) shear walls are one of the common lateral load resisting elements in buildings in seismic regions. They are commonly used both in civil and industrial buildings and in power plant buildings. As a matter of fact, the walls, thanks to their dimensions and in-plane disposition, give a high stiffness and a high resistance to the building, reducing the inter-storey drift values at damage limit state and providing enough strength and ductility at collapse.

Shear walls can, based on their geometry, be divided into two groups, high-rise and low-rise shear walls. High rise shear walls, also called slender walls, are governed by flexural behaviour (as underlined in [1] and [2]). On the other hand, low-rise walls, also called squat walls, characterized by a ratio of height to length less than or equal to two are governed by shear behaviour (as demonstrated in [3]).

RC shear walls are commonly designed to satisfy criteria of serviceability and safety. In order to ensure the serviceability requirement, it is necessary to predict the cracking and the deflections of RC walls under service loads. In order to assess the margin of safety of RC walls against failure an accurate estimation of the ultimate load is essential and the prediction of the load-deformation behaviour of the structure throughout the range of elastic and inelastic response is desirable. Within the framework of achieving a wider understanding of all mechanical phenomena associated with the elastic and, particularly, inelastic behaviour of RC walls, experimental research still plays a very important role. Moreover, experimental research supplies the information needed for the development of advanced design methods, such as nonlinear finite element analysis (NLFEA).

The scientific research has therefore made significant advancements in understanding the nonlinear behaviour of RC walls subjected to horizontal forces and several numerical methods have been developed and tailored to analyse such kind of structural member. In particular, in this paper, the focus is pointed on the assessment of RC squat walls by means of NLFEA and multi-layered shell elements. In order to investigate the prediction capacity and to reduce the uncertainties related to of NLFE tools, round robin competitions and blind prediction were recently organized and are in progress nowadays (e.g. Concrack2 benchmark [4], SMART-2013 [5], CASH benchmark [6], etc.)

In this paper the results obtained analysing the squat walls object of the CASH benchmark is presented. The main objective of this benchmark is to evaluate the seismic nonlinear response of squat walls, representative of a real nuclear power plant (NPP) building structure. According to the purpose of the benchmark, three different kind of analyses have been carried out: pushover, cyclic and dynamic analysis.

NLFEA are carried out using the PARC_CL 2.0 crack model. The PARC_C 2.0 crack model was implemented, by the authors of this paper, within the ABAQUS code as a user subroutine UMAT.for. Such model is an evolution of the previous PARC versions [7]-[8] and allows to consider plastic and irreversible deformation in the unloading phase. Moreover, the implementation, within the PARC_CL 2.0 crack model, of a formulation able to account for stiffness proportional damping allows the possibility to apply it for dynamic analyses.

2 THE PARC_CL 2.0 CRACK MODEL

In this paper the nonlinear mechanical behaviour of reinforced concrete was achieved by means of PARC_CL 2.0 crack model. The PARC_CL 2.0 (Physical Approach for Reinforced Concrete under Cyclic Loading) crack model is an evolution of the previous PARC versions ([7] and [8]) and allows considering plastic and irreversible deformation in the unloading

phase and therefore to take into account the hysteretic cycles of both concrete and steel reinforcement. Moreover, in order to proper analyse the dynamic behaviour, the Rayleigh damping stiffness-proportional coefficient was developed and introduced within the PARCL_CL 2.0 crack model. For further details on PARC_CL 2.0 implementation please refers to [9] and [10].

2.1 Fixed crack approach

The proposed PARC_CL 2.0 model is based on a total strain fixed crack approach, in which at each integration point two reference systems are defined: the local *x,y*-coordinate system and the orthotropic *1,2*-coordinate system along the principal stress directions. The angle between the *1*-direction and the *x*-direction is denoted as ψ, whereas θ_i is the angle between the direction of the *i*th order of the bar and the *x*-direction. When the value of the principal tensile strain in concrete exceeds the concrete tensile limit strain $\varepsilon_{t,cr}$, for the first time, the first crack is formed and the *1,2*-coordinate system is fixed, Figure 1-a.

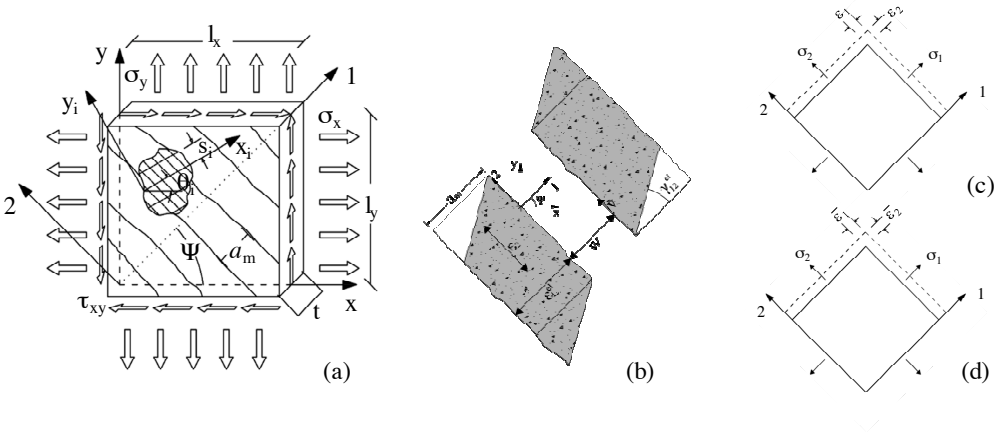

Figure 1 – (a) RC element subjected to plane stress conditions, (b) crack parameters, (c) biaxial strain condition (d) uniaxial strain condition.

2.1.1. Strain Field for Concrete

The concrete behaviour is assumed orthotropic both before and after cracking and the total strains at each integration point are calculated in the orthotropic *1,2*-system, Figure 1-a:

$$\left\{\varepsilon_{1,2}\right\} = \left[T_\psi\right] \cdot \left\{\varepsilon_{x,y}\right\} \tag{1}$$

where $\left[T_\psi\right]$ is the transformation matrix, shown in Eq.(2):

$$\left[T_\psi\right] = \begin{bmatrix} \cos^2\psi & \sin^2\psi & \cos\psi \cdot \sin\psi \\ \sin^2\psi & \cos^2\psi & -\cos\psi \cdot \sin\psi \\ -2\cdot\cos\psi\cdot\sin\psi & 2\cdot\cos\psi\cdot\sin\psi & \cos^2\psi - \sin^2\psi \end{bmatrix} \tag{2}$$

$\{\varepsilon_{1,2}\}$ and $\{\varepsilon_{x,y}\}$ represent respectively the biaxial strain vector in *1,2*-system and *x,y*-system, as shown in Eq.(3) and Eq.(4), Figure 1-c.

$$\left\{\varepsilon_{1,2}\right\} = \left\{\varepsilon_1 \quad \varepsilon_2 \quad \gamma_{12}\right\}^t \tag{3}$$

$$\left\{\varepsilon_{x,y}\right\} = \left\{\varepsilon_x \quad \varepsilon_y \quad \gamma_{xy}\right\}^t \tag{4}$$

The stress-strain behaviour presented herein is calculated on the base of the uniaxial strains in the *1,2*-coordinate system, calculated according to Eq.(5), Eq.(6) and Eq.(7), and shown in Figure 1-d.

$$\bar{\varepsilon}_1 = \frac{1}{1-\nu^2}\varepsilon_1 + \frac{\nu}{1-\nu^2}\varepsilon_2 \tag{5}$$

$$\bar{\varepsilon}_2 = \frac{\nu}{1-\nu^2}\varepsilon_1 + \frac{1}{1-\nu^2}\varepsilon_2 \tag{6}$$

$$\bar{\gamma}_{12} = \gamma_{12} \tag{7}$$

After the first crack the Poisson's ratio is assumed to be zero therefore in Eq.(5), Eq.(6) and Eq.(7), the biaxial strains are the same as the uniaxial strains. This condition is illustrated in Figure 1-b and Figure 1-c, where the stresses σ_1 and σ_2 are related to the uniaxial strains and represent both the biaxial stresses and the uniaxial stresses.

2.1.2. Strain Field for Steel

The reinforcement is assumed smeared in concrete. The steel strain along the reference system of each bar are obtained rotating the strains in the *x,y*-system, it is possible to obtain the uniaxial strains along each steel bars, as follow:

$$\varepsilon_{xi} = \varepsilon_x \cos^2\theta_i + \varepsilon_y \sin^2\vartheta_i + \gamma_{xy}\cos\theta_i \sin\theta_i \tag{8}$$

2.1.3. Stress Field for Concrete

The concrete stress vector, in the *1,2*-coordinate system can be generated as follow:

$$\left\{\sigma_{1,2}\right\} = \left\{\sigma_1 \quad \sigma_2 \quad \tau_{12}\right\}^t = \left\{\sigma_{1,2}\right\}_{static} + \left\{\sigma_{1,2}\right\}_{dynamic} \tag{9}$$

where σ_1 and σ_2 represent the stresses in concrete in the normal directions, while τ_{12} is the shear stress in concrete. All these values are derived as the sum of the "static" contribute, $\{\sigma_{1,2}\}_{\text{static}}$ described in §2.2, and the "dynamic" contribute, $\{\sigma_{1,2}\}_{\text{dynamic}}$ described in §2.3.

2.1.4. Stress Field for Steel

The steel stress vector, defined for each *i*th order of bar in the x_i,y_i-coordinate system, can be generated as follow:

$$\left\{\sigma_{x_i,y_i}\right\} = \left\{\sigma_{x_i} \quad 0 \quad 0\right\}^t = \left\{\sigma_{x_i,y_i}\right\}_{static} + \left\{\sigma_{x_i,y_i}\right\}_{dynamic} \tag{10}$$

where σ_{xi} represents the stress along the axis of the *i*th order of bar and it can be calculated as the sum of the "static" contribute, $\{\sigma_{xi,yi}\}_{\text{static}}$ described in §2.2, and the "dynamic" contribute, $\{\sigma_{xi,yi}\}_{\text{dynamic}}$ described in §2.3. From Eq.(10) it can be noted that no stresses in the direction perpendicular to the axis of the bar develop, due to the fact that the dowel action phenomenon has not been considered yet.

2.1.5. Total Stress Field

Both the concrete and the steel stress vectors can be transformed from their local coordinate system to the overall global *x*,*y* coordinate system using respectively Eq.(11) and Eq.(12):

$$\left\{\sigma_{x,y}\right\}_c = \left[T_\psi\right]^t \cdot \left\{\sigma_{1,2}\right\} \tag{11}$$

$$\left\{\sigma_{x,y}\right\}_{s,i} = \left[T_{\theta i}\right]^t \cdot \left\{\sigma_{x_i,y_i}\right\} \tag{12}$$

where $\left[T_\psi\right]^t$ and $\left[T_{\theta i}\right]^t$ are the transpose of the transformation matrixes, already reported in Eq.(2).

The total stress in the *x*,*y*-system is obtained by assuming that concrete and reinforcing bars behave like two springs placed in parallel:

$$\left\{\sigma_{x,y}\right\} = \left\{\sigma_{x,y}\right\}_c + \sum_{i=1}^{n} \rho_i \left\{\sigma_{x,y}\right\}_{s,i} \tag{13}$$

where n is the total number of the orders of bars and ρ_i represents the reinforcement ratio for every ith order of bars.

2.2 Static cyclic behaviour

The concrete and steel behaviours as well as their interaction effects are modelled with constitutive relationships for loading-unloading-reloading conditions. The hysteretic response for concrete and steel subjected to static cyclic loading is briefly described in this section, for further details please refers to [9] and [10].

2.2.1. Concrete model

The envelope curve for concrete, shown in Figure 2-a, is defined by Eq.(14) for tensile behaviour and Eq.(15) for compressive behaviour.

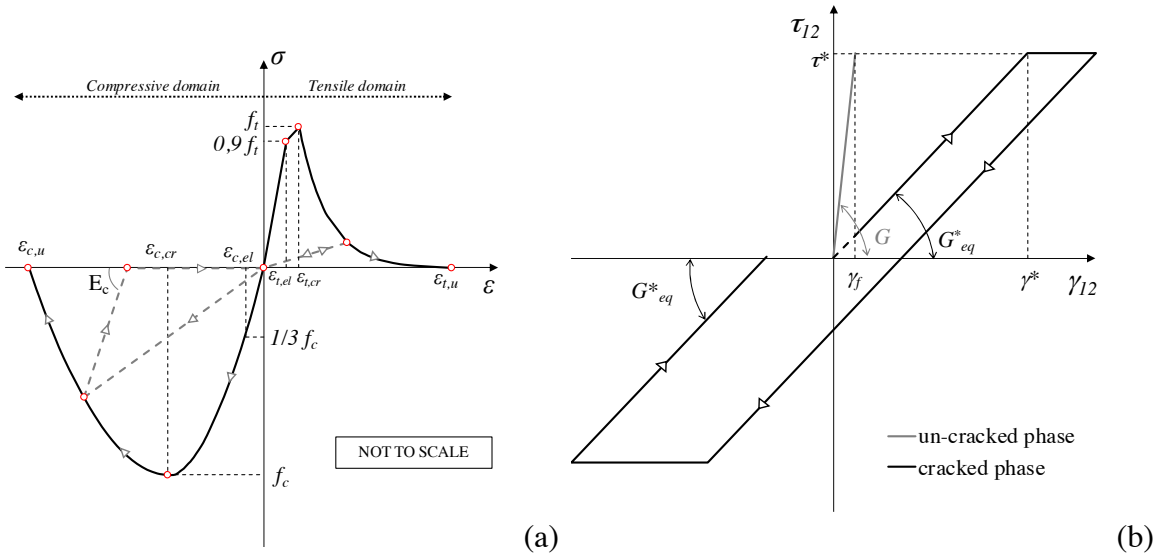

Figure 2 – Hysteretic response of concrete: (a) normal behaviour and (b) shear behaviour.

$$\sigma = \begin{cases} E_c \cdot \varepsilon & 0 \le \varepsilon < \varepsilon_{t,el} \\ 0.9 \cdot f_t + 0.1 \cdot f_t \left(\dfrac{\varepsilon - \varepsilon_{t,el}}{\varepsilon_{t,cr} - \varepsilon_{t,el}} \right) & \varepsilon_{t,el} \le \varepsilon < \varepsilon_{t,cr} \\ f_t \left\{ \left[1 + \left(c_1 \cdot \dfrac{\varepsilon - \varepsilon_{t,cr}}{\varepsilon_{t,u}} \right)^3 \right] \cdot \exp\left(- c_2 \cdot \dfrac{\varepsilon - \varepsilon_{t,cr}}{\varepsilon_{t,u}} \right) - \dfrac{\varepsilon - \varepsilon_{t,cr}}{\varepsilon_{t,u}} \cdot \left(1 + c_1^{\,3} \right) \cdot \exp\left(- c_2 \right) \right\} & \varepsilon_{t,cr} \le \varepsilon < \varepsilon_{t,u} \\ 0 & \varepsilon \ge \varepsilon_{t,u} \end{cases} \tag{14}$$

$$\sigma = \begin{cases} E_c \cdot \varepsilon & \varepsilon_{c,el} < \varepsilon \le 0 \\ \dfrac{f_c}{3} \cdot \left[1 + 4 \cdot \left(\dfrac{\varepsilon - \varepsilon_{c,el}}{\varepsilon_{c,cr} - \varepsilon_{c,el}} \right) - 2 \cdot \left(\dfrac{\varepsilon - \varepsilon_{c,el}}{\varepsilon_{c,cr} - \varepsilon_{c,el}} \right)^2 \right] & \varepsilon_{c,cr} < \varepsilon < \varepsilon_{c,el} \\ f_c \cdot \left[1 - \left(\dfrac{\varepsilon - \varepsilon_{c,cr}}{\varepsilon_{c,u} - \varepsilon_{c,cr}} \right)^2 \right] & \varepsilon_{c,u} < \varepsilon < \varepsilon_{c,cr} \\ 0 & \varepsilon \le \varepsilon_{c,u} \end{cases} \tag{15}$$

where:

$\varepsilon_{t,el} = 0.9 \cdot f_t / E_c$ $\quad \varepsilon_{t,cr} = 0.00015$ $\quad \varepsilon_{t,u} = 5.136 \cdot G_F / (a_m \cdot f_t)$ $\quad c_1 = 3$

$\varepsilon_{c,el} = f_c / (3 \cdot E_c)$ $\quad \varepsilon_{c,cr} = 5 \cdot \varepsilon_{c,el}$ $\quad \varepsilon_{c,u} = \varepsilon_{c,cr} - 1.5 \cdot G_C / (a_m \cdot f_c)$ $\quad c_2 = 6.93$

The value of h in the PARC_CL 2.0 crack model is fixed equal to the square root of the average element area, according to [12].

The value of G_F represents the fracture energy of concrete in tension and can be evaluated according to [13]. The value of G_F is defined as the energy required to propagate a tensile crack in a unit area of concrete. The transition between the dissipated energy by a single macro-crack in concrete, G_F, and the energy dissipated by several macro-crack in reinforced concrete, G_F^{RC}, is defined in accord with Eq.(16):

$$G_F^{RC} = G_F \left(1 + \frac{h}{a_m} \right) \tag{16}$$

where a_m is set as the average crack spacing and can be calculated on the base of the length over which the sleep between concrete and steel occurs, $l_{s,max}$, as define in [14]. G_C represents the fracture energy of concrete in compression. The ratio between the fracture energy of concrete in compression and in tension is assumed equal to 250 according to [15].

As shown in Figure 2-a the cyclic behaviour for concrete along the orthotropic *1,2*-directions is defined with a slope secant to the origin for the tensile domain, on the other hand, the compressive cyclic domain is characterized by an unloading branch with slope E_c.

Multi-axial state of stress is considered by reducing the compressive strength and the corresponding peak strain due to lateral cracking, as given in Eq. (17), according to [16].

$$\zeta = 1 \Big/ \left(0.85 - 0.27 \, \varepsilon_{\perp} \Big/ \varepsilon \right) \quad 0.4 \le \zeta \le 1 \tag{17}$$

where ε represents the current compressive strain of concrete and $\varepsilon_{\perp}$ is the tensile strain.

The shear behaviour along the crack is accounted in the model considering the aggregate interlock phenomenon, on the base of the formulation proposed in [17]. The overall τ_{12}-γ_{12} behaviour, shown in Figure 2-b, can be derived as reported in Eq.(18), on the base of the crack width, w, and the crack sliding, v.

$$\tau_{12} = \begin{cases} G \cdot \gamma_{12} & \text{if } \gamma_{12} \le \gamma_f \\ \dfrac{\tau^*}{\gamma^*} \cdot \gamma_{12} = G^*_{eq} \cdot \gamma_{12} & \text{if } \gamma_f < \gamma_{12} \le \gamma^* \\ \tau^* & \text{if } \gamma_{12} > \gamma^* \end{cases} \tag{18}$$

where γ_f corresponds to the shear strain at the onset of concrete cracking and γ^* defines the point after which the shear strain remains constant and is equal to:

$$\gamma^* = \gamma^*_{cr} + \gamma_f \tag{19}$$

According to the formulation proposed in [17] the main parameters of Eq.(18) and Eq.(19) can be calculated as follow:

$$\tau^* = \bar{\tau} \cdot \left(1 - \sqrt{\frac{2\,w}{d_{\max}}} \right) \frac{a_3 + a_4 \left| \dfrac{v^*}{w} \right|^3}{1 + a_4 \left(\dfrac{v^*}{w} \right)^4} \frac{1}{w} v^* \tag{20}$$

$$\gamma^*_{cr} = \frac{v^*}{h} \tag{21}$$

where $\bar{\tau} = 0.27 \cdot f_c$; $v^* = \dfrac{f_c}{a_5} w + a_6$; $a_3 = \dfrac{2.45}{\bar{\tau}}$; $a_4 = 2.44 \left(1 - \dfrac{4}{\bar{\tau}} \right)$; $a_5 = 0.366 \cdot f_c + 3.333$ and $a_6 = f_c / 110$

The cyclic behaviour of the shear contribution is also taken into account by considering, in the unloading phase, a branch with slope G^*_{eq}, as shown in Figure 2-b.

2.2.2. Steel model

The constitutive relation for steel, employed in PARC_CL 2.0 crack model, is based on the formulation proposed in [18] and allows to represent the hysteretic stress-strain behaviour of reinforcing steel bar also including yielding, strain hardening and Bauschinger effect, Figure 3.

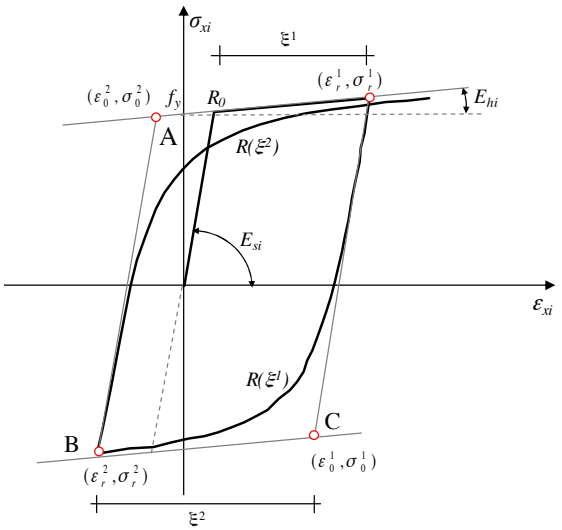

Figure 3 – PARC_CL 2.0, cyclic behaviour of reinforcing steel.

The formulation proposed in [18] and shown in Figure 3 can be expressed following Eq.(22):

$$\sigma_{xi} = \sigma^* \cdot (\sigma_0 - \sigma_r) + \sigma_r \tag{22}$$

where:

$$\sigma^* = b \cdot \varepsilon^* + \frac{(1-b)\varepsilon^*}{\left(1+\varepsilon^{*R}\right)^{1/R}} \tag{23}$$

$$\varepsilon^* = \frac{\varepsilon_{xi} - \varepsilon_r}{\varepsilon_0 - \varepsilon_r} \tag{24}$$

The presented equations represent a curved transition from a straight line asymptote with E_{si} inclination to another asymptote with E_{hi} inclination, Figure 3. In Eq.(22) and Eq.(24), σ_0 and ε_0 represent the stress and the strain in the point where the two asymptotes of the considered branch meet (e.g. point A in Figure 3); similarly σ_r and ε_r are the stress and the strain in the point where the last strain reversal occurs (e.g. point B in Figure 3). As indicated in Figure 3, (σ_0,ε_0) and (σ_r,ε_r) are updated at each strain reversal; b is the strain-hardening ratio and can be calculated as the ratio between E_{hi} and E_{si}:

Finally, R is the parameter that influences the shape of the transition curve between the two asymptotes and allows a good representation of Bauschinger effect. R is considered dependent on the strain difference between the point in which the last strain reversal occurs (e.g. point B in Figure 3 for the considered branch) and the previous asymptotes meeting point (e.g. point C in Figure 3 for the considered branch). The expression of R is reported in Eq.(25):

$$R = R_0 - \frac{a_1 \cdot \xi}{a_2 + \xi} \tag{25}$$

where R_0 is the value of the parameter R during the first loading cycle, a_1 and a_2 are experimentally determined parameters. Based on the parametric studies carried out in [10], in this paper these parameters are set equal to: R_0=20, a_1=18.45 and a_2=0.001.

2.3 Dynamic behaviour

The energy dissipation associated to the material modelling was considered in the PARC_CL 2.0 crack model by introducing the stiffness proportional Rayleigh damping, according to the following general equation:

$$\sigma_{dynamic} = \beta \cdot E' \cdot \dot{\varepsilon} \tag{26}$$

Based on Eq.(26) the "dynamic" contribution of Eq.(9) and Eq.(10) can be derived as expressed in Eq.(27) and Eq.(28) for concrete and steel respectively:

$$\left\{\sigma_{1,2}\right\}_{dynamic} = \begin{Bmatrix} \beta \cdot E'_{c1} \cdot \dot{\varepsilon}_1 \\ \beta \cdot E'_{c2} \cdot \dot{\varepsilon}_2 \\ \beta \cdot G'_{12} \cdot \dot{\gamma}_{12} \end{Bmatrix} \tag{27}$$

$$\left\{\sigma_{x_i,y_i}\right\}_{dynamic} = \begin{Bmatrix} \beta \cdot E'_{si} \cdot \dot{\varepsilon}_{xi} \\ 0 \\ 0 \end{Bmatrix} \tag{28}$$

2.4 Consistent tangent Jacobian matrix

The proposed PARC_CL 2.0 crack model is based on a tangent approach except in softening branches where the stiffness contributes of concrete became to avoid numerical problems. As already shown for the evaluation of the stresses vectors, also the Jacobian matrix can be subdivided in "static" and "dynamic" terms.

Regarding the "static" term the Jacobian matrix can be expressed as the derivative of the stresses with respect to the strains as shown in Eq.(29) for concrete and in Eq.(30) for each *i*th order of bars:

$$\left[D_{1,2}\right]_{static} = \begin{bmatrix} \dfrac{\partial \sigma_1}{\partial \varepsilon_1}\dfrac{1}{\left(1-\nu^2\right)} & \dfrac{\partial \sigma_1}{\partial \varepsilon_2}\dfrac{\nu}{\left(1-\nu^2\right)} & 0 \\ \dfrac{\partial \sigma_2}{\partial \varepsilon_1}\dfrac{\nu}{\left(1-\nu^2\right)} & \dfrac{\partial \sigma_2}{\partial \varepsilon_2}\dfrac{1}{\left(1-\nu^2\right)} & 0 \\ 0 & 0 & \dfrac{\partial \tau_{12}}{\partial \gamma_{12}} \end{bmatrix} \tag{29}$$

$$\left[D_{x_i,y_i}\right]_{static} = \begin{bmatrix} \dfrac{\partial \sigma_{xi}}{\partial \varepsilon_{xi}} & 0 & 0 \\ 0 & 0 & 0 \\ 0 & 0 & 0 \end{bmatrix} \tag{30}$$

The "dynamic" term of the Jacobian matrix can be evaluate as the derivative of the "dynamic" stresses, already reported in Eq.(26) with respect to the strains.

$$\frac{d\sigma_{damp}}{d\varepsilon} = \beta \cdot E' \cdot \frac{1}{dt} \tag{31}$$

where *dt* denotes the increment of time.

Considering that the Jacobian matrix for "static" contribution, already reported in Eq.(29) for concrete and Eq.(30) for steel, contains itself the tangent stiffness modulus, *E'*, the Jacobian tangent stiffness matrix related to the "dynamic" contribution can be express as in Eq.(32) for concrete and in Eq.(33) for steel:

$$\left[D_{1,2}\right]_{dynamic} = \left[D_{1,2}\right]_{static} \cdot \left(\beta \cdot \frac{1}{dt}\right) \tag{32}$$

$$\left[D_{x_i,y_i}\right]_{dynamic} = \left[D_{x_i,y_i}\right]_{static} \cdot \left(\beta \cdot \frac{1}{dt}\right) \tag{33}$$

The overall Jacobian matrix can be calculated as the sum of static and dynamic contribution, as reported in Eq.(34) for concrete and Eq.(35) for steel:

$$\left[D_{1,2}\right] = \left[D_{1,2}\right]_{static} + \left[D_{1,2}\right]_{dynamic} = \left[D_{1,2}\right]_{static} \cdot \left(1 + \beta \cdot \frac{1}{dt}\right) \tag{34}$$

$$\left[D_{x_i,y_i}\right] = \left[D_{x_i,y_i}\right]_{static} + \left[D_{x_i,y_i}\right]_{dynamic} = \left[D_{x_i,y_i}\right]_{static} \cdot \left(1 + \beta \cdot \frac{1}{dt}\right) \tag{35}$$

Finally, the global stiffness matrix is obtained from Eq.(36):

$$\left[D_{x,y}\right] = \left[T_{\psi}\right]^t \cdot \left[D_{1,2}\right] \cdot \left[T_{\psi}\right] + \sum_{i=1}^{n} \rho_i \left[T_{\theta i}\right]^t \cdot \left[D_{x_i,y_i}\right] \cdot \left[T_{\theta i}\right] \tag{36}$$

In order to validate the proposed model and to assess its capability to predict the damping effect on a RC member, a comparison between NLFEA and analytical formulation is presented.

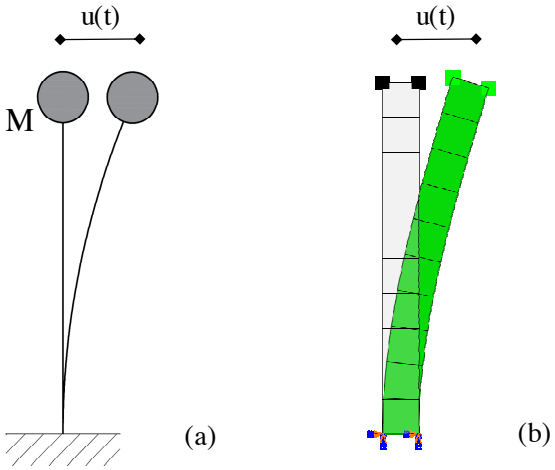

Figure 4 – Free vibration oscillator: (a) SDF analytical system and (b) NLFE model.

A Single Degree of Freedom (SDF) system, represented by the cantilever tower of Figure 4-a, was used as a reference system. The cantilever tower is characterized by a section of 100x100 mm and a height of 1000 mm. The system is fixed at the base and it presented a lumped mass at the top equal to 50 Kg. The elastic modulus of the material was set equal to 28000 MPa. NLFEA was carried out in order to assess the proposed damping model in the PARC_CL2.0 crack model. The same cantilever tower, representing a SDF system, reported in Figure 4-a was modelled by means of NLFEA as shown in Figure 4-b.

The height of the tower was subdivided into 10 shell elements with 4 nodes and 4 Gauss integration points (defined S4 in ABAQUS code [11]), so each element presents a 100x100 mm size in plane. The thickness of each element was set equal to 100 mm in order to achieve the same cross section as the reference analytical specimen. The two nodes at the base of the tower were fixed and at the top of the tower two mass elements of 25 Kg were added.

In order to highlight the frequency of the numerical system, a frequency analysis was carried out before running the dynamic analysis. The frequency analysis highlight that the first vibration mode, able to excite the 99.4% of the mass, presents a frequency, $f=19.7\ Hz$, so that the corresponding natural frequency was equal to $\omega=123.8\ Hz$.

According to the Rayleigh damping formulation, the damping ratio can be written as a function of the mass proportional coefficient, α, and the stiffness proportional coefficient, β, as shown in Eq.(37).

$$\xi_n = \frac{\alpha}{2} \cdot \frac{1}{\omega_n} + \frac{\beta}{2} \cdot \omega_n \tag{37}$$

Due to the fact that the analysed system presents a single degree of freedom, it was necessary only a single frequency to calibrate the damping coefficient. In order to validate the stiffness-proportional damping introduced in the PARC_CL 2.0 crack model, only the stiffness-proportional damping coefficient, β, was calculated. Thus, in Eq.(37) the α coefficient was set equal to 0 while the β coefficient was calculated based on the natural frequency, ω, and the damping ratio, ξ.

The NLFE model was firstly subjected to a horizontal displacement at the top of the specimen equal to 0.01 mm. In a second phase the system was released to experience free vibration in dynamic field. The time step was set equal to 0.0005 sec and the numerical solution is obtained by means of the Newmark's implicit method considering average acceleration.

In Figure 5 the comparison between NLFEA and analytical formulation for different values of damping ratio are presented.

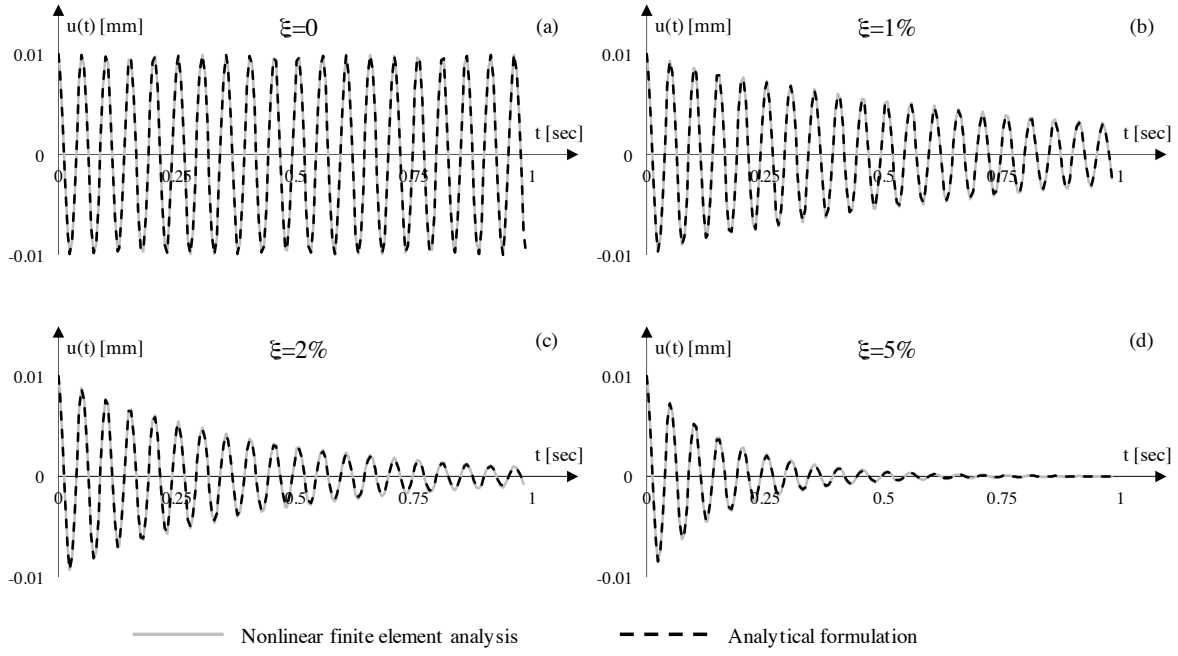

Figure 5 – Free vibration, comparison between NLFEA and analytical formulation for different values of damping ratio: (a) un-damped system, (b) ξ=1%, (c) ξ=2% and (d) ξ=5%.

The results reported in Figure 5 show that the stiffness-proportional damping introduced in the PARC_CL 2.0 crack model allows to reproduce well the dissipation of energy due to damping in a linear elastic system.

3 EXPERIMENTAL CAMPAIGN

The proposed PARC_CL 2.0 crack model was used to analyse the monotonic, cyclic and dynamic response of RC squat walls by means of NLFEA. This study is included within the CASH benchmark project [19], which is an international benchmarking program organized under an initiative of the OEDC-NEA (Nuclear Energy Agency). The main objective of the benchmark was to evaluate the reliability of NLFEA to assess the seismic capacity of RC squat walls, by means of comparison with experimental outcomes. The experimental reference case is based on the "SAFE" RC squat walls tested at the European Laboratory for Structural Assessment (ELSA, Joint Research Centre) [20]. The SAFE experimental campaign consists of a series of pseudo-dynamic (PSD) tests on 13 different squat walls, with different reinforcement ratio representative of the nuclear industry practice. In particular, for the purpose of this paper, 3 out of the 13 specimens was selected: T6 [21], T7 [22] and T8 [23]specimen.

All the specimens have the same geometrical properties: a length l = 3000 mm a height h = 1200 mm and a thickness t = 200 mm. In order to reproduce the effect of perpendicular walls, at both the ends of each specimen two flanges were added. The top and the bottom part of the specimen are made of rigid concrete beams, as shown in Figure 6-a.

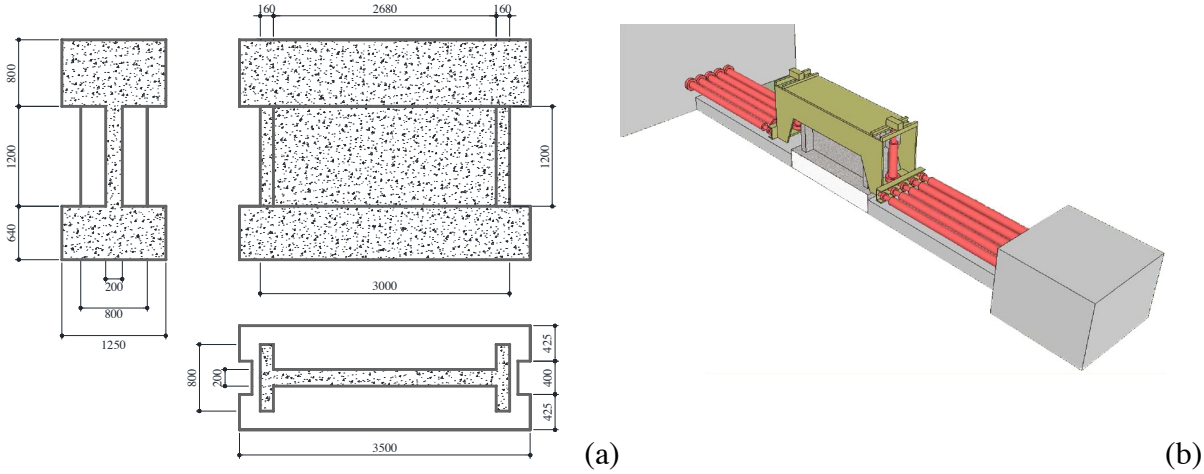

Figure 6 – (a) Geometrical properties of all the analysed specimens (measure in mm) and (b) experimental set-up [19].

In order to apply pure shear to the specimen the rotation of the top beam was constrained with two vertical jacks and the steel cover presented in Figure 6-b.

The differences in the specimens are in percentage of steel, ρ, in vertical compressive stress, σ_n, in the numerical mass applied in the PSD test, M_2, and in the first vibration frequency, f. The mean mechanical properties of the specimens are listed in Table 1. In Table 1 the mass M_1 represents the physical mass of the top beam including the steel cover, the mass M_2 represents the numerical mass applied in the PSD test, N the vertical load imposed at the top beam of each specimen and σ_n the vertical stress due to the combination of self-weight and imposed vertical load.

Table 1 - Mechanical and geometrical properties of all the specimens.

Spec.	Masses		Load		Concrete			Horizontal Reinforcement				Vertical Reinforcement			
	M_1	M_2	N	σ_v	f_c	f_t	E_c	ρ_h	f_y	E_S	ϕ	ρ_v	f_y	E_S	ϕ
	[ton]	[ton]	[kN]	[MPa]	[MPa]	[MPa]	[GPa]	[%]	[MPa]	[GPa]	[mm]	[%]	[MPa]	[GPa]	[mm]
T6	25	1252	550	1.01	33.1	3.1	22.3	0.628	573	200	10	0.402	594	200	8
T7	25	11272	550	1.01	36.4	3.3	23.1	0.628	573	200	10	0.402	594	200	8
T8	25	1252	550	0.32	28.6	2.8	21.3	0.402	594	200	8	0.402	594	200	8

The modulus of elasticity of concrete was not directly obtained by tests but was derived adopting the formulation proposed in [14], Eq.(38):

$$E_{C,MC2010} = 21500 \cdot \left(\frac{f_c}{10} \right)^{1/3} \tag{38}$$

Consequently, assuming a Poisson's ratio equal to 0.2 the conventional isotropic shear modulus for concrete, G, could be derived. The analytical shear stiffness of the wall, K_A, is evaluated with Eq.(39):

$$K_A = \frac{G \cdot (b \cdot t)}{h} \tag{39}$$

where b, t, h represent the base, the thickness and the height of the wall, respectively.

Finally, knowing the mass of each wall, M, (considered as the sum of physical mass, M_1, and numerical mass, M_2), the frequency of the wall could be analytically derived. The analytical calculation of the main features of the specimens are listed in Table 2 with the subscript A. Prior to run the experimental PSD tests, the eigenfrequency of each specimen, f_{exp}, was measured by low level vibration and the corresponding elastic stiffness, K_{exp}, was derived. The obtained experimental results and the comparison with the analytical values are also reported in Table 2.

Table 2 – Main features of the specimens: comparison between analytical calculation and experimental results.

Specimen	b	h	t	$E_{c,MC2010}$	G	M_1+M_2	Analytical		Experimental		K_{exp}/K_A
							K_A	f_A	K_{exp}	f_{exp}	
	[m]	[m]	[m]	[MPa]	[MPa]	[ton]	[MN/m]	[Hz]	[MN/m]	[Hz]	[MPa]
T6	3	1.2	0.2	31900	13292	1277	6649	11.6	5348	10.4	0.80
T7	3	1.2	0.2	32900	13708	11297	6861	3.9	5767	3.6	0.84
T8	3	1.2	0.2	30400	12667	1277	6336	11.3	4557	9.6	0.72
									Average		0.79

Interestingly, from Table 2 it appears that the analytically calculated stiffness significantly overestimates the measured one. The average value of the ratio between the experimental and the analytical stiffness is equal to 0.79, close to the 0.7 median value obtained by [24]. According to the results of these preliminary studies in the NLFEA, the modulus of elasticity of concrete was reduced by a factor 0.7 with respect to the one calculated according to Eq.(38). In Table 1 the adopted elastic modulus is reported as E_c.

4 NONLINEAR FINITE ELEMENT ANALYSIS

NLFEA have been carried out with ABAQUS code [11] adopting the PARC_CL 2.0 crack model. Each element is characterized by 4 Gauss integration points (S4) in plane while, along the thickness, it is divided in 2 layers with 3 Simpson section integration points.

The pushover analyses are limited to T6 and T8 specimens; in particular, for each specimen three different mesh configurations are analysed, characterized by an average element size of 200 mm (coarse mesh), 100 mm (medium mesh) and 50 mm (fine mesh), Figure 7. The aim of this analyses was to investigate the capability of the proposed method to minimize the mesh dependency effect.

The same specimens are analysed also for static cyclic analyses in order to compare the obtained hysteretic response with the experimental results; for the static cyclic analyses only the fine mesh, characterized by an average element length of 50 mm, was investigated.

The dynamic analyses are limited to T6 and T7 specimens, in order to highlight the influence of the numerical applied mass which strongly changes the frequency of the specimen; for the dynamic analyses only the fine mesh, characterized by an average element length of 50 mm, was adopted.

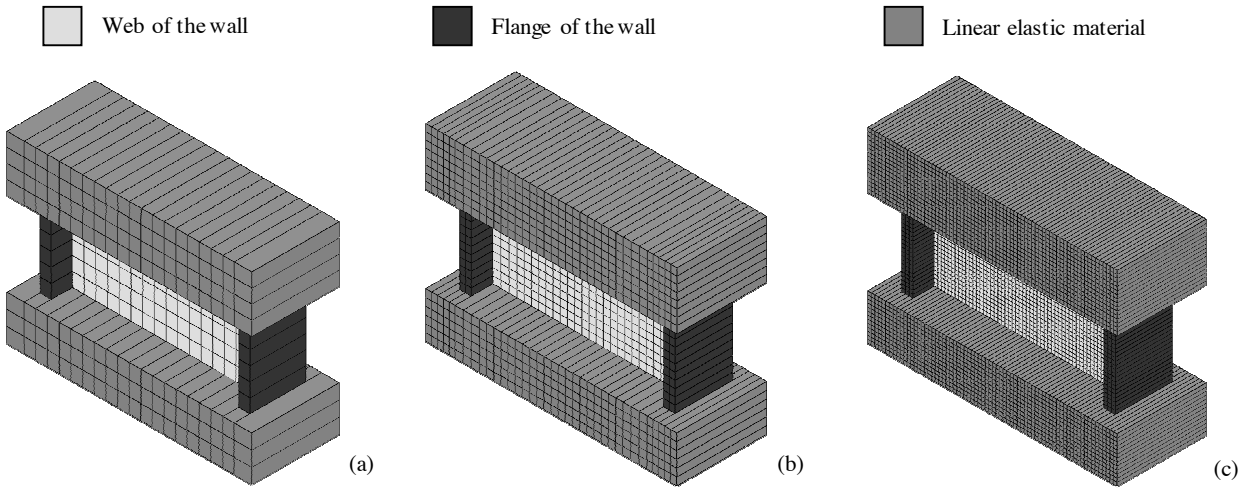

Figure 7 – Solid view of the meshes adopted for NLFEA: (a) coarse mesh, (b) medium mesh and (c) fine mesh.

The top and the bottom beams was modelled using linear elastic material, while the web and the two flanges of the wall were modelled using PARC_CL 2.0 crack model. Furthermore, due to the confining effect of stirrups, the flanges are modelled considering a confined concrete, calculated according to the formulation proposed by [25], which leads to an increase of both the compressive strength and the ultimate compressive strain. The analyses have been carried out using the mean values of the material properties as reported in Table 3.

The boundary and loading conditions applied for static pushover and cyclic analyses are presented in Figure 8-a. The translation in the *x*-direction is fixed in correspondence of the anchor elements of the experimental specimens; the translation along the *z*-direction is fixed at the base of the bottom beam and the out-of-plane behaviour is prevented by fixing the translation along the *y*-direction of the whole model. Load is applied in two different steps: in the first step the self-weight and the vertical pressure are applied; in the second step the horizontal displacement is imposed in correspondence of the "Sec T" section, Figure 8-a. During the experimental tests, in order to apply pure shear condition to the wall, the rotation of the top beam was prevented by means of two vertical jacks. In NLFEA the same condition is obtained by applying a multi-point constraint in "Sec T". The pushover analyses have been car-

ried out increasing the horizontal displacement until the failure. The cyclic analyses have been carried out applying to "Sec T" the horizontal displacement measured during the experimental PSD tests, Figure 8-a. The implicit method was adopted by the solver, while the Newton-Raphson method was used as convergence criterion. The force and displacement tolerance was fixed to $5 \cdot 10^{-3}$ for forces and 10^{-2} for displacements.

Table 3 – Main mechanical properties used in NLFE model.

Spec.	Mesh	Concrete (see §2.2.1.)														Steel (see §2.2.2.)		
								un-confined				confined						
		h	a_m	Ec	f_t	G^{RC}_F	$\varepsilon_{t,u}$	f_c	G_C	$\varepsilon_{c,cr}$	$\varepsilon_{c,u}$	f_c	G_C	$\varepsilon_{c,cr}$	$\varepsilon_{c,u}$	E_s	$f_{y,vert}$	$f_{y,hor}$
		[mm]	[mm]	[GPa]	[MPa]	[N/mm^3]	[-]	[MPa]	[N/mm^3]	[-]	[-]	[MPa]	[N/mm^3]	[-]	[-]	[GPa]	[MPa]	[MPa]
T6	Coarse	200	245	22.3	3.1	0.155	0.002	33.1	38.8	0.002	0.011	38.9	88.1	0.003	0.019	200	594	572
	Medim	100	245	22.3	3.1	0.120	0.003	33.1	30.0	0.002	0.016	38.9	56.6	0.003	0.025	200	594	572
	Fine	50	245	22.3	3.1	0.103	0.005	33.1	25.8	0.002	0.025	38.9	40.9	0.003	0.034	200	594	572
T7	Medium	100	245	23.0	3.3	0.103	0.002	36.4	25.8	0.002	0.013	39	58.2	0.003	0.026	200	594	572
T8	Coarse	200	288	21.3	2.8	0.131	0.002	28.6	32.8	0.002	0.011	34	74.4	0.003	0.019	200	594	594
	Medim	100	288	21.3	2.8	0.104	0.003	28.6	26.0	0.002	0.016	34	48.4	0.003	0.024	200	594	594
	Fine	50	288	21.3	2.8	0.091	0.005	28.6	22.8	0.002	0.026	34	35.4	0.003	0.035	200	594	594

For the dynamic analysis the boundary conditions were the same for pushover analysis, while load is applied in different manner, Figure 8-b. An additional numerical mass, acting only along x-direction, defined as M_2 in Table 1, is added in the centroid of the top beam to simulate the numerical mass of the experimental tests. As for pushover analysis the load is applied in two different steps: in a first step the self-weight and the vertical pressure is applied; in a second step the horizontal acceleration is imposed and the rotation of the top beam is prevented by applying a multi-point constraint, which imposes the same vertical displacements of the central node of "Sec T" to all the other nodes of "Sec T", Figure 8. In dynamic analysis the structural damping was introduced according to Rayleigh's classical theory defined in Eq.(37). The mass proportional term (α) is introduced as an input value in the ABAQUS code [11], while the stiffness proportional term (β) was incorporated in the PARC_CL 2.0 crack model as explained in §2.3. The α and β Rayleigh's damping coefficients, according to the CASH benchmark organizer (that is the organizer of the project within which these analyses are carried out [Le Corvec et al., 2015]), are calibrated in order to obtain a damping ratio of 2% for the frequencies of 0.5Hz and 35 Hz.

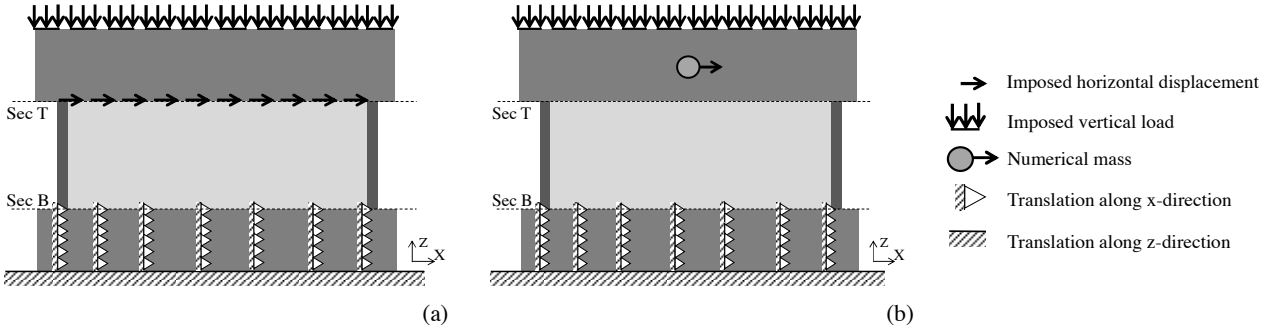

Figure 8 – Boundary and loading conditions adopted for NLFEA: (a) static pushover and cyclic analyses and (b) dynamic analysis.

4.1 Static pushover analysis

In Figure 9 the comparison between the experimental results and the static pushover analysis, in terms of shear-force vs top displacement, for T6 and T8 specimens, is presented. As just stated, in order to highlight the effect of the mesh dependency three different meshes are analysed: a coarse mesh with an average element size of 200 mm, a medium mesh with an average element size of 100 mm and a fine mesh with an average element size of 50 mm.

In Figure 9 the analyses are stopped when the failure occurred, due to crushing of concrete. Crushing of concrete is achieved when the compressive strain of concrete reaches the ultimate value, $\varepsilon_{c,u}$, shown in Figure 10 and Figure 11 for T6 and T8 specimen respectively. The values of $\varepsilon_{c,u}$, for the different meshes analysed, are reported in Table 3.

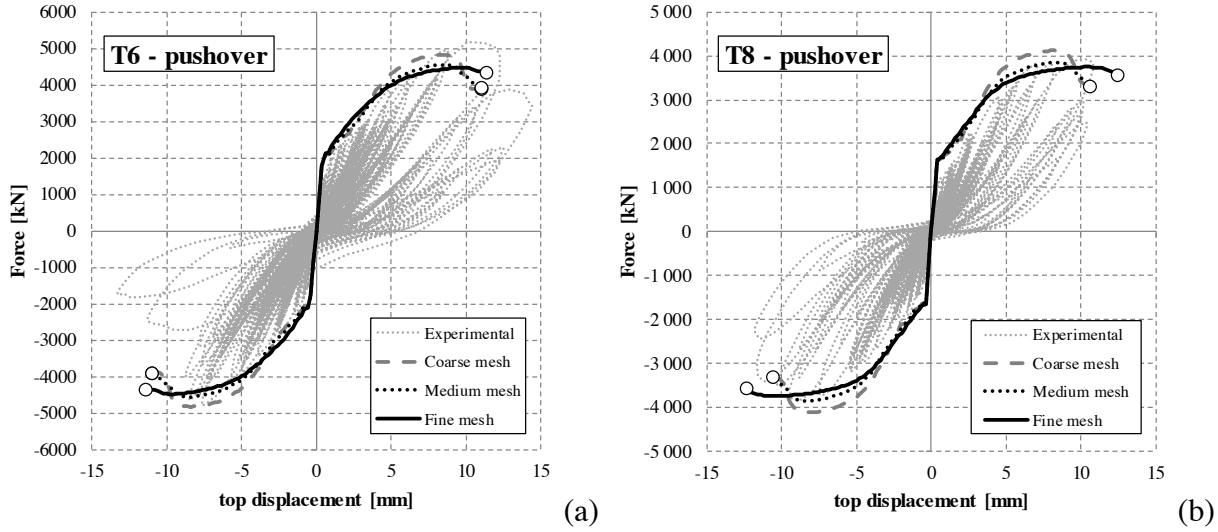

Figure 9 – Static pushover analysis, T6 wall: effect of using meshes with different average element size.

The curves reported in Figure 9 showed that the results obtained analysing the same specimen with different meshes are quite similar; so, it can be assess that the idea to modify the fracture energy of concrete as a function of the element length and crack spacing can avoid the mesh dependency effects. Finally, in Figure 10 and Figure 11 the contours representing the crushing of concrete are reported for T6 and T8 specimen respectively.

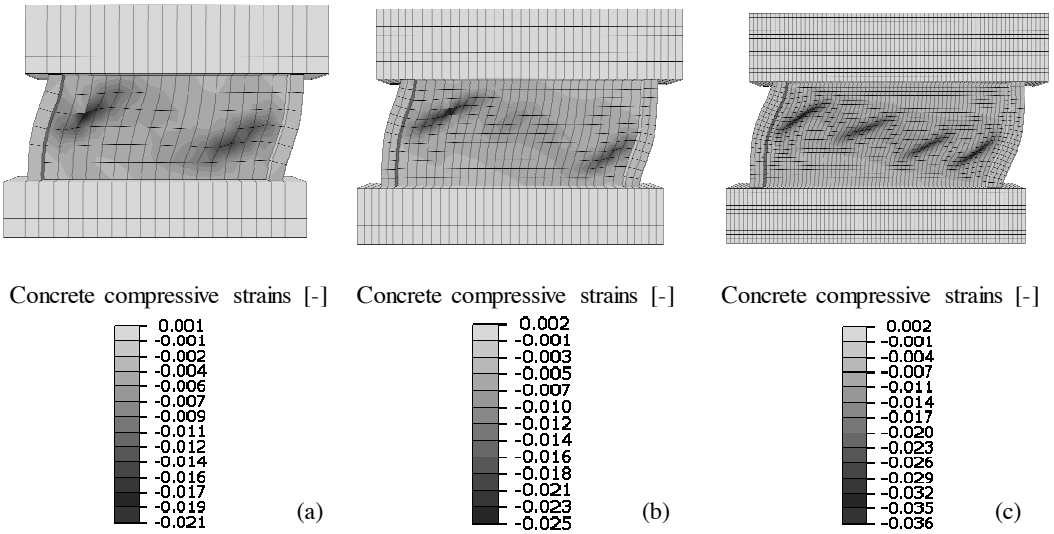

Figure 10 – Static pushover analysis of T6 wall, crushing of concrete for the different analysed meshes using PARC_CL 2.0 crack model: (a) coarse mesh, (b) medium mesh and (c) fine mesh.

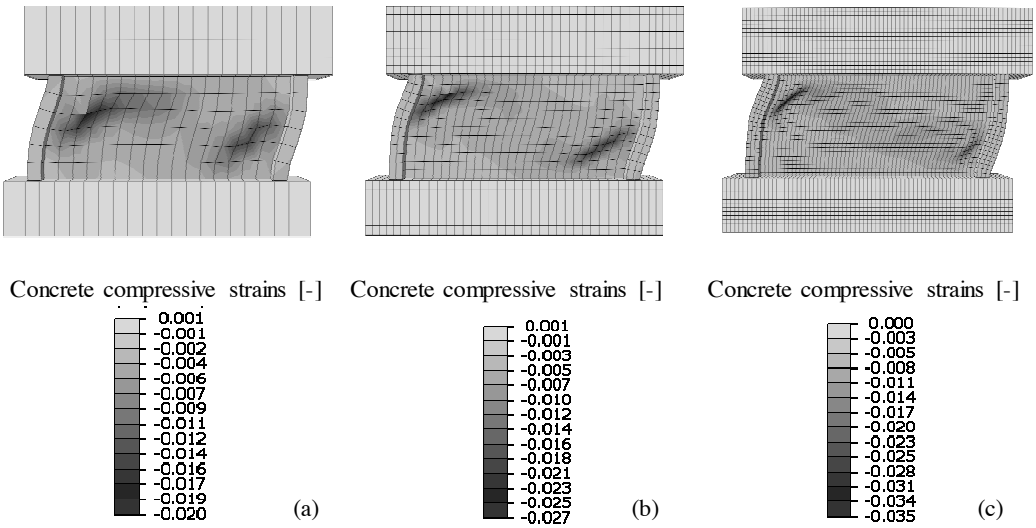

Figure 11 – Static pushover analysis of T8 wall, crushing of concrete for the different analysed meshes using PARC_CL 2.0 crack model: (a) coarse mesh, (b) medium mesh and (c) fine mesh.

Figure 9 highlights that using different meshes it is possible to obtain similar results in term of shear strength and failure mode. For the following static cyclic and dynamic analyses, the fine mesh characterized by an average element size of 50 mm is chosen.

4.2 Static cyclic analysis

In Figure 12 are presented the results of the static cyclic analysis obtained for T6 and T8 specimens with NLFEA using the PARC_CL 2.0 crack model together with the experimental outcomes.

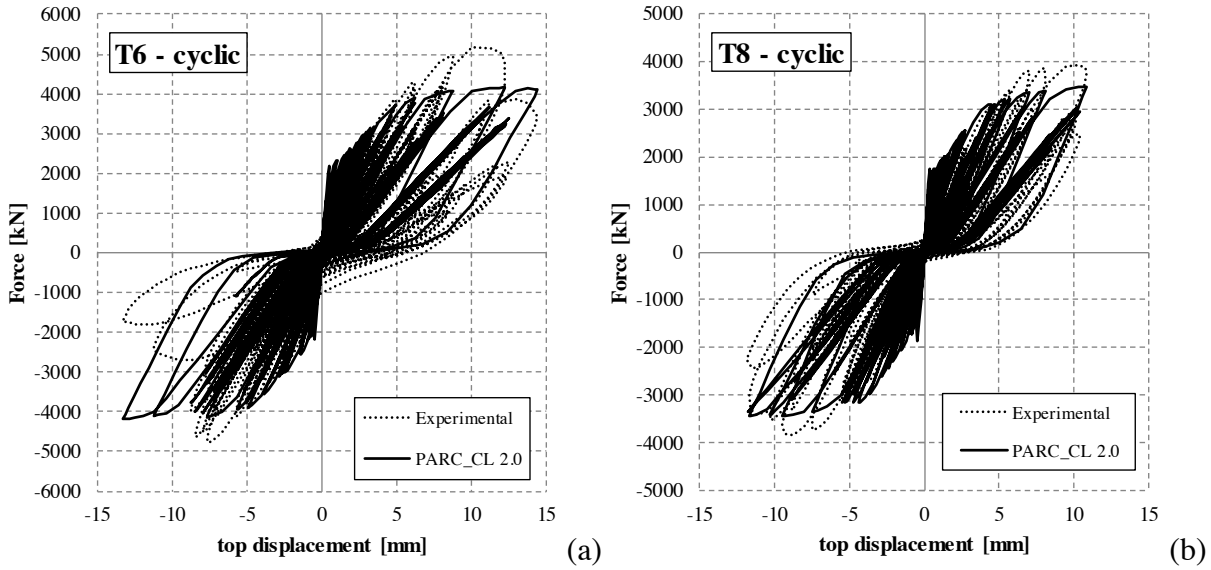

Figure 12 - Static cyclic analysis of T6 wall: comparison of experimental results with NLFEA using PARC_CL 2.0 and PARC_CL 1.0 crack models.

Figure 12 clearly shows that NLFEA carried out using the PARC_CL 2.0 crack model are able to reproduce the hysteretic response experimentally obtained. From Figure 12 it can be also highlight that the results obtained by means of NLFEA presented, as expected, a symmetric shape with respect to the origin, due to the fact that the specimen is perfectly symmetric in

geometric and loading condition. On the other hand, the experimental results for T6 specimen, Figure 12-a, presents an higher strength value on the positive displacement side.

In this context, it has to be remarked that the imposed cyclic displacement, derived by the measured displacement in the experimental PSD test, did not yield the specimens, both T6 and T8, to failure. However, analysing the results of the pushover analysis, presented above, and of the dynamic analysis, presented in the following, it can be expected that a small increasing of the imposed displacement could bring the specimen up to crushing failure.

4.3 Dynamic analysis

In this section dynamic time history analyses of T6 and T7 specimens are carried out; these two specimens, neglecting the little differences in the concrete mechanical properties, differ only in the numerical mass applied in the Pseudo-Dynamic experimental test, as shown in Table 1. This difference can strongly influence the frequency of the system; for this reason, before running the full dynamic time history analyses, the frequency analyses have been carried out in order to calculate the natural frequency of each specimen and to compare it with the experimental results.

Table 4 – Natural frequency and elastic stiffness: comparison between LFEA and experimental.

		NLFEA		Experimental		
Specimen	M [ton]	f_{NLFEA} [Hz]	K_{NLFEA} [MN/m]	f_{exp} [Hz]	K_{exp} [MN/m]	$\frac{f_{NLFEA}}{f_{exp}}$
T6	1252	9.6	4551	10.4	5341	0.92
T7	11272	3.4	5139	3.6	5761	0.94
				Average		0.93

From Table 4 it could be seen how the natural frequency obtained by means of NLFEA, f_{NLFEA}, is close to the experimental one. Indeed, the average value of the ratio between numerical and experimental frequency is equal to 0.93.

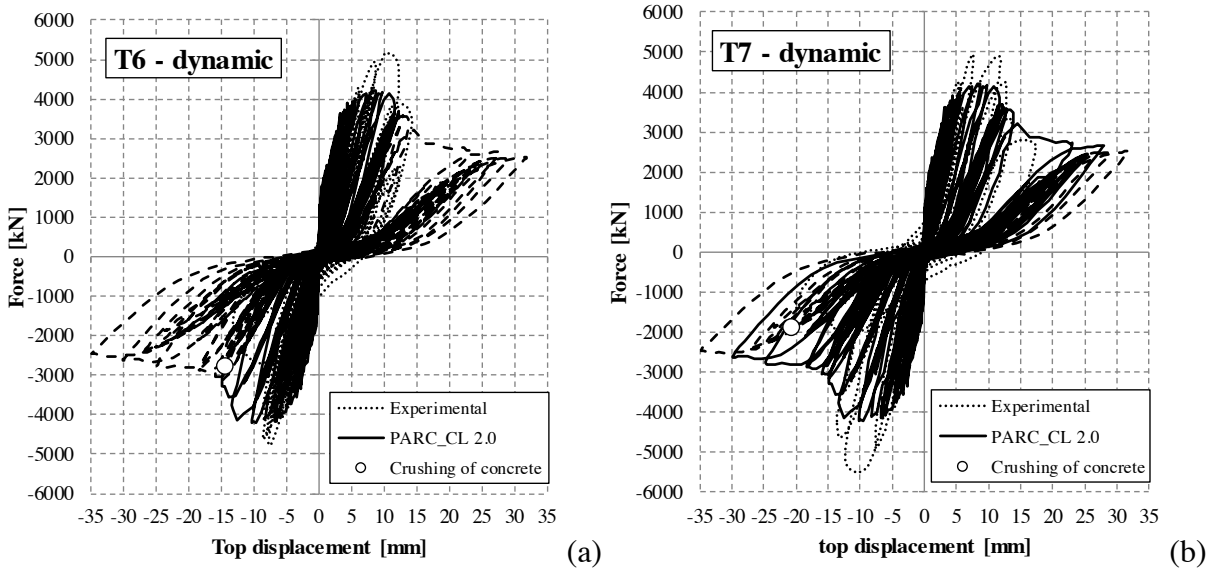

Figure 13 – Dynamic time histories analyses: comparison between experimental outcomes and NLFEA with PARC_CL 2.0 crack model for (a) T6 specimen and (b) T7 specimen.

Finally, in Figure 13 the results obtained with dynamic time history analyses are plotted and compared with the results of the experimental Pseudo-Dynamic tests.

In Figure 13 the point corresponding to the crushing of concrete, and so to the failure of the specimen, is marked; after the crushing of concrete is reached, the NLFEA curve is presented with a dotted line. The crushing of concrete in NLFEA is considered as the point in which concrete reaches the ultimate strain, $\varepsilon_{c,u}$, reported in Table 3 (remember that for dynamic analysis the fine mesh is used).

Comparing Figure 13-a with Figure 13-b it appears that for T6 specimen the crushing of concrete occurs before than for the T7 specimen. Indeed, for T6 specimen the crushing of concrete occurs after 33.2 seconds out of the 74.4 seconds of the analysis, while for T7 specimen the crushing of concrete occurs after 64.5 seconds out of the 74.4 seconds of the analysis.

In order to underline the capability of the PARC_CL 2.0 crack model to reproduce the hysteretic response of the analysed specimens, in Figure 14 the comparison between NLFEA and experimental results is reported. The NLFE curves are stopped when the crushing of concrete is reached.

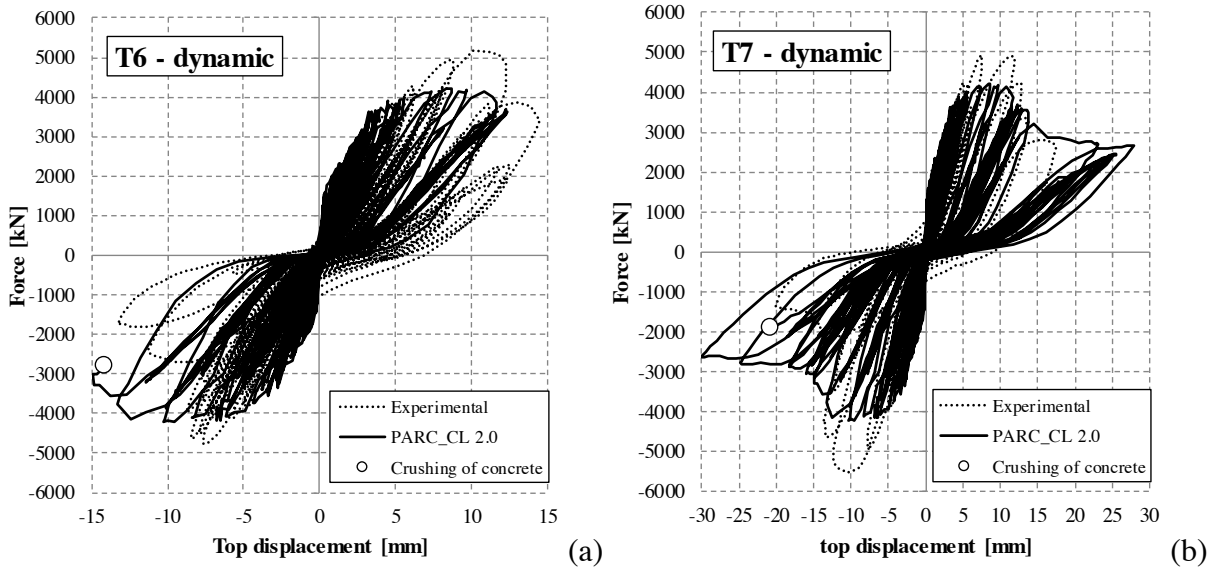

Figure 14 – Dynamic time histories analyses stopped after the crushing of concrete: comparison between experimental outcomes and NLFEA with PARC_CL 2.0 crack model for (a) T6 specimen and (b) T7 specimen.

From Figure 14 it can be remarked that the PARC_CL 2.0 crack model are able to reproduce the hysteretic behaviour of reinforced concrete squat walls subjected to dynamic loading.

5 CONCLUSIONS

In this paper the monotonic, cyclic and dynamic behaviour of RC squat walls was investigated by means of NLFEA carried out using multi-layer shell elements and the implemented PARC_CL 2.0 crack model. The main conclusions can be remarked as follow:

- The definition of a fracture energy for reinforced concrete, G_F^{RC}, allows to avoid the mesh dependency effect; indeed, the pushover analyses carried out using three different meshes (coarse mesh, medium mesh and fine mesh) lead to comparable results;
- The PARC_CL 2.0 crack model seems to well reproduce the cyclic behaviour of a RC squat walls, in particular it was highlighted that, a proper definition of the hysteretic behaviour of concrete and steel leads to well reproduce the structural cyclic response, not only in the loading phase but also in the unloading phase;
- The implementation, within the PARC_CL 2.0 crack model, of the stiffness proportional Rayleigh damping allows to run dynamic time history analyses. The results ob-

tained using NLFEA and PARC_CL 2.0 are able to predict the cyclic behaviour of such kind of structural member. Nevertheless, further studies are needed to refine the dynamic model.

REFERENCES

[1] *Belletti B., Damoni C., Gasperi A.* (2013) Modeling approaches suitable for pushover analyses of RC structural wall buildings. Engineering Structures, 57(12): 327-338

[2] Scolari M., Belletti ., Vecchi F. (2017) In-plane and out-of-plane cyclic response prediction of RC structural walls by means of multi-layered shell elements and PARC_CL 2.0 crack model. Submitted to Engineering Structures.

[3] *Damoni C., Belletti B., Esposito R.* (2014). Numerical prediction of the response of a squat shear wall subjected to monotonic loading. European Journal of Environmental and Civil Engineering, 18(7): 754-769;

[4] *Concrack2* (2011). 2nd Workshop on Control of Cracking in RC structures. 2011. CEOS.fr reserach programme, 2011, Paris, France.

[5] *Richard B., Fontan M., Mazars J.*, (2014). Smart 2013: overview, synthesis and lessons learnt from the international benchmark. Ref: SEMT/EMSI/NT/14-037, Document émis dans le cadre de l'accord bipartite CEA-EDF.

[6] *Le Corvec V., Petre-Lazar I., Lambert E., Gallitre E., Labbe P., Vezin J.M., Ghavamian S.*, (2015). CASH benchmark on the beyond design seismic capacity of reinforced concrete shear walls, Proceedings of SMiRT23 Conference, 10-14 August 2015, Manchester (United Kingdom).

[7] *Belletti, B., Cerioni R., and Iori* I. (2001). Physical approach for reinforced-concrete (PARC) membrane elements. ASCE Journal of Structural Engineering, 127(12), pp. 1412-1426.

[8] *Belletti B., Esposito R., Walraven J.* (2013). Shear Capacity of Normal, Lightweight, and High-Strength Concrete Beams according to ModelCode 2010. II: Experimental Results versus Nonlinear Finite Element Program Results. ASCE Journal Of Structural Engineering, 139(9), pp. 1600-1607.

[9] *Belletti B., Scolari M., Vecchi F.* (2017) PARC_CL 2.0 crack model for NLFEA of reinforced concrete structures under cyclic loadings. Submitted to Computers and Structures.

[10] *Scolari M.,* (2016). Implementation of PARC_CL 2.0 crack model for reinforced concrete members subjected to cyclic and dynamic loading, Ph.D. thesis, University of Parma

[11] *Abaqus 6.12* (2012). User's and Theory Manuals 2012. http://www.3ds.com/.

[12] *Hendriks, M.A.N., Uijl J.A, De Boer, A.,. Feenstra, P.H., Belletti, B., Damoni, C.* (2012). "Guidelines for nonlinear finite element analyses of concrete structures", Rijkswaterstaat Technisch Document (RTD), Rijkswaterstaat Centre for Infrastructure, RTD:1016:2012.

[13] *fib – International Federation for Structural Concrete* (1993). fib-Model Code 1990. (MC90), Thomas Telford, London.

[14] *fib – International Federation for Structural Concrete*. (2010). fib Model Code for Concrete Structures 2010. Berlin: Verlag Ernst & Sohn, 2013.

[15] *Nakamura, H., and Higai, T*. (2001). "Compressive fracture energy and fracture zone length of concrete." Modeling of inelastic behavior of RC structures under seismic loads, P. Benson Shing and T. Tanabe, eds., ASCE, Reston, VA, 471–487.

[16] *Vecchio F. J., Collins M. P.,* (1993). "Compression response of cracked reinforced concrete", Journal of Structural Engineering, ASCE, 119 (12), 1993, pp. 3590-3610.

[17] *Gambarova P. G.,* (1983). "Sulla trasmissione del taglio in elementi bidimensionali piani di C.A. fessurati", Proc., Giornate AICAP, 1983, pp141–156 (in Italian).

[18] *Menegotto M., Pinto, P.E*. (1973). "Method of analysis for cyclically loaded R.C. plane frames including changes in geometry and non-elastic behaviour of elements under combined normal force and bending, Symposium on the Resistance and Ultimate Deformability of Structures Acted on by Well Defined Repeated Loads", International Association for Bridge and Structural Engineering, (ABSE) Lisbon, Portugal.

[19] *Le Corvec V., Petre-Lazar I., Lambert E., Gallitre E., Labbe P., Vezin J.M., Ghavamian S.,* (2015). CASH benchmark on the beyond design seismic capacity of reinforced concrete shear walls, Proceedings of SMiRT23 Conference, 10-14 August 2015, Manchester (United Kingdom).

[20] *Pegon P*. (1998). Programme SAFE: Présentation générale des essais, *JRC technical note*.

[21] Pegon P., Magonette G., Molina F.J., Verzeletti G., Dyngeland T., Negro P., Tirelli D., Tognoli P., (1998[a]). 'Programme SAFE: rapport du test T6' JRC technical note.

[22] *Pegon P., Magonette G., Molina F.J., Verzeletti G., Dyngeland T., Negro P., Tirelli D., Tognoli P.,* (1998[b]). 'Programme SAFE: rapport du test T7' JRC technical note.

[23] *Pegon P., Magonette G., Molina F.J., Verzeletti G., Dyngeland T., Negro P., Tirelli D., Tognoli P.,* (1998[c]). 'Programme SAFE: rapport du test T8' JRC technical note.

[24] *Sozen M.A., Moehle J.P*. (1993), Stiffness of Reinforced Concrete Walls Resisting In Plane Shear, Report No. EPRI TR-102731 Electric Power Research Inst., Palo Alto (CA).

[25] *Mander, J., Priestley, M., and Park, R*. (1988). "Theoretical Stress-Strain Model for Confined Concrete.", J. Struct. Eng., 10.1061/(ASCE)0733-9445(1988)114:8(1804), 1804-1826.